# Computational analysis of vibrational frequencies and rovibrational spectroscopic constants of hydrogen sulfide dimer using MP2 and CCSD(T)

João B.L. Martins [a,*], Rabeshe P. Quintino [a], José R. dos S. Politi [a], Daniel Sethio [b], Ricardo Gargano [c], Elfi Kraka [b]

[a] Institute of Chemistry, University of Brasília, Brasília, DF 70910-900, Brazil
[b] Computational and Theoretical Chemistry Group (CATCO), Department of Chemistry, Southern Methodist University, 3215 Daniel Avenue, Dallas, TX 75275-0314, United States
[c] Institute of Physics, University of Brasília, Brasília, DF 70910-900, Brazil

## ARTICLE INFO

## ABSTRACT

Previous studies have shown that the weakly bonded $H_2S$ dimer demands high level quantum chemical calculations to reproduce experimental values. We investigated the hydrogen bonding of $H_2S$ dimer using MP2 and CCSD(T) levels of theory in combination with aug-cc-pV(*D,T,Q*)Z basis sets. More precisely, the binding energies, potential energy curves, rovibrational spectroscopic constants, decomposition lifetime, and normal vibrational frequencies were calculated. In addition, we introduced the local mode analysis of Konkoli-Cremer to quantify the hydrogen bonding in the $H_2S$ dimer as well as providing for the first time the comprehensive decomposition of normal vibrational modes into local modes contributions, and a decomposition lifetime based on rate constant. The local mode force constant of the $H_2S$ dimer hydrogen bond is smaller than that of the water dimer, in accordance with the weaker hydrogen bonding in the $H_2S$ dimer.

© 2020 Elsevier B.V. All rights reserved.

## 1. Introduction

Investigation of weak intermolecular interactions is of critical concern in many fields, including physics, astronomy, materials, chemistry, and biology [1–19]. The nature of these weak interactions provides an unambiguous field for high level *ab initio* standards [20–22]. Accordingly, there have been numerous studies of $H_2O$ dimer compared to the $H_2S$ dimer [23–25]. Consequently, the experimental and theoretical features of $H_2O$ dimer interactions are far advanced. However, because of the critical role of $H_2S$ intermolecular interactions, the accurate assessment of $H_2S$ hydrogen bonding has been widely explored [6,22,26–29]. Indeed, several outstanding contributions to the theoretical study of vibrational frequencies of $H_2S$ dimer were reported [21,22,27–32]. From these studies, a relevant compilation with prior experimental and theoretical results of binding energies, zero point energy (ZPE), and structural parameters is available [21].

Hydrogen bonding in water has been investigated in a wide range of approaches, where the infrared spectra are an important source for the knowledge of weak to strong hydrogen bond. The most prominent effect is regarding the red shift of X-H⋯Y stretching mode, where anharmonic coupling between low and high frequency modes was studied beyond the adiabatic approximation [33–40], and the resonance between the first excited state and two high frequencies, the Davydov coupling [39].

*Ab initio* potential energy surfaces (PES) for water dimer are a great effort in spectroscopic studies [25,41–52]. However, tractable full 12D nuclear motion is a challenge. These are useful for fitting *ab initio* PES with the Terahertz vibration-rotation tunneling (VRT) spectroscopic data, where accurate PES are needed. Examples include the SAPT level that was used to generate SAPT-5s water pair potential [41] by fitting 2510 interaction energies associated to 6D frozen monomer, and accurately predict the water dimer spectra with an uncertainty of 0.3 kcal/mol for the interaction energy [41]. The VRT (MCY-5f) potential dependent on 12 degrees of freedom was based in water monomer flexibility to address the prediction of tunneling frequencies [45]. The spectroscopic accuracy was achieved, despite the intramolecular infrared shifts been less satisfactory [45]. Vibrationally averaged VRT spectra were obtained for the water dimer with evaluation of 12D potential energy [46] with $>10^{12}$ geometries, leading to a modest improvement of VRT states for water dimer low-lying vibration-rotation tunneling states [46]. CCSD(T) based pair potential (CC-pol) for water was developed using the 2510 grid points of SAPT-5s potential, and the complete 6D potential surface shows an uncertainty of 0.07 kcal/mol for the interaction energy [47]. CC-pol prediction of rotational constants, tunneling splitting and vibrational frequencies presents the lowest RMS values compared with experimental data of 2.1%, 12% and 4.4%, respectively [47]. Fully

coupled 6D water dimer VRT levels show sensitive to the shape of anharmonic potentials [48]. _Ab initio_ 12D potential (CCpol-8sf) with flexible monomers for water dimer lead to the correct binding energy, equilibrium geometry and frequency difference < 2 cm$^{-1}$ [49]. Therefore, we are conscious that using rigid motions for monomer modes has to be addressed with special concern and cautiousness for the spectroscopic analysis, as shown by the literature for the VRT splittings associated with weakly bound dimer.

It is well known that one of the main concerns in the $H_2S$ fundamental frequencies is the separation between symmetric ($\nu_1 = 2614.4$ cm$^{-1}$) and antisymmetric ($\nu_3 = 2628.4$ cm$^{-1}$) stretching modes, which is reported as 14 cm$^{-1}$ [6,53–57]. In addition to this small band separation, the issue of weak absorption complicates the investigation of its infrared spectrum [6,58]. Other behavior of impact is that $H_2S$ aggregates easily in low-temperature matrix experiments forming dimers and higher oligomers [6,28], and in this case, the hydrogen bond in the $H_2S$ dimer was recently confirmed by microwave spectroscopy [27].

$H_2S$ dimer infrared modes have been studied in solid Ne [32], Ar [58–60], Kr [58,59], Xe [58], $N_2$ [59,61], and $O_2$ [62], and the reported stretching modes are in the range of 2572.5 to 2581.5 cm$^{-1}$. Most recently, the $H_2S$ dimer was studied in the gas phase with vacuum ultraviolet ionization-detected IR-predissociation spectroscopy [28]; where the S—H ($\nu_{S-H}^b$) of the H-bond donating $H_2S$ was assigned to a frequency of 2590 cm$^{-1}$ corresponding to a redshift of 31 cm$^{-1}$ obtained in relation to the free $H_2S$ molecule. This redshift is smaller than that found for O—H of $H_2O$ dimer (106 cm$^{-1}$) [63]. The second frequency of 2605 cm$^{-1}$ was assigned to the symmetric S—H stretch of the acceptor $H_2S$ moiety ($\nu_1^a$). However, the disagreement is within the peak appearing at 2618 cm$^{-1}$, it was explained as an overlap of free S—H of H-bond donor and the antisymmetric mode of the acceptor moiety ($\nu_3^a$) [6,58]. In the same way, Fourier transform infrared spectroscopy was applied to hydrogen sulfide in solid neon [32], and follows the same trend. The donor S—H ($\nu_{S-H}^b$) was assigned to the 2596.5 cm$^{-1}$ band with intensity of 100 km/mol, and the symmetric S—H ($\nu_1^a$) at 2605.0 cm$^{-1}$ with intensity of 25 km/mol. However, Soulard and Tremblay showed that both $\nu_3$ signatures at 2622.1 cm$^{-1}$ (intensity of 10 km/mol) could not be clearly attributed to the proton donor or acceptor [32].

Theoretical and experimental studies have investigated the structural parameters and vibrational frequencies of the weak interaction in $H_2S$ dimer [21–42,44–53,64–73]. Dreux and Tschumper [22] carried out high level optimizations at different levels of theory including CCSD(T)/ha(Q + d)Z with anharmonic correction to the MP2 harmonic. Lemke [21] performed CCSD(T)/aug-cc-pVQZ (aQZV) harmonic and anharmonic studies of $H_2S$ dimer, along with a Complete Basis Set (CBS) limit study. The harmonic stretching frequencies from CCSD(T)/ aVQZ are 2729, 2726, 2714 and 2691 cm$^{-1}$, while the extrapolated MP2 anharmonic frequencies are 2629, 2627, 2615, and 2615 cm$^{-1}$ [21]. These two studies are the most recent theoretical results and will be used as standards.

The study of weak interactions has developed remarkably in recent decades thanks to the progress made, both in experimental techniques generally based on the use of cross molecular beams, spectroscopy and laser, and in the theoretical methodologies of the calculation of potential energy curves (PECs) [74–76]. The modeling of these systems based on the first principles is a source of understanding of fundamental trends and behaviors.

The major goal of this study was to quantify and characterize the intrinsic strength of the hydrogen bonds in the $H_2S$ dimer using local vibrational force constants derived local vibrational modes and to decompose the vibrational spectrum in local mode contributions to characterize the normal vibrational modes. These local vibrational modes were precisely assigned to the bonds and interactions found in this dimer. The local mode analysis was complemented by the calculation and analysis of dimer PEC as well as the discussion of

spectroscopic constants, rovibrational energies, and decomposition lifetime.

## 2. Computational details

We have studied the $H_2S\cdots H_2S$ interaction at the MP2, and CCSD(T) levels of theory, where the correlation consistent aug-cc-pV(_D,T,Q_)Z (hereafter referred to as aVDZ, aVTZ, and aVQZ, respectively) basis sets were used. MP2 calculations were carried out using the Gaussian16 Rev B.01 [77] computational program. All coupled cluster calculations were performed with the CFOUR program version 2.00 beta [78]. Equilibrium geometries and analytical harmonic vibrational frequencies were obtained using the MP2 and CCSD(T). MP2 anharmonic corrections were obtained from second-order vibrational perturbation theory (VPT2), while for CCSD(T) anharmonic corrections were obtained using the MP2 anharmonic frequencies. Binding energies ($D_e$) were calculated for the equilibrium geometry. It is well known that stabilization energy values of weakly linked molecular complexes are overestimated due to the fact that each monomer has influence from the basis set that describes the other monomer, resulting in artificial and overestimated stabilization. This overestimation is known as the basis set superposition error (BSSE). To correct for BSSE, the Boys–Bernardi counterpoise (CP) procedure for the final geometry was utilized. In addition, zero point energy (ZPE) was also considered for the contributions of vibrational energy at absolute zero.

### 2.1. Local mode analysis and characterization of normal mode procedure

Computational methods frequently model the strength of a chemical bond through molecular orbital approaches [79,80], dissociation energies [81–83], or energy decomposition methods [84,85]. Through the years, these approaches provide more qualitative rather than quantitative results [86,87]. To address this gap in theory, we utilized local vibrational force constants based on the local mode analysis of Konkoli and Cremer [87–89] to quantify the intrinsic strength of the S-H$\cdots$S interaction responsible for H–S donor, acceptor and S$\cdots$H bond.

### 2.2. Local vibrational modes and associated local mode properties

In 1998, Konkoli and Cremer [89,90] derived for the first time local vibrational modes directly from normal vibrational modes by solving the mass-decoupled Euler-Lagrange equations, i.e. by solving the local equivalent of the Wilson equation of vibrational spectroscopy [91,92]. They developed the leading parameter principle [89,90] which states that for any internal, symmetric, curvilinear, etc., coordinate a local mode $\mathbf{a}_n$ can be defined. $\mathbf{a}_n$ is independent of all other internal coordinates used to describe the geometry of a molecule, which also means that it is also independent of using redundant or non-redundant coordinate sets. The local mode vector $\mathbf{a}_n$ associated with the $n$-th internal coordinate $q_n$ is defined as [89,90].

$$\mathbf{a}_n = \frac{\mathbf{K}^{-1}\mathbf{d}_n^\dagger}{\mathbf{d}_n\mathbf{K}^{-1}\mathbf{d}_n^\dagger}, \tag{1}$$

where the local mode $\mathbf{a}_n$ is expressed in terms of normal coordinates $\mathbf{Q}$, the diagonal matrix $\mathbf{K}$ contains the normal mode force constants, and $\mathbf{d}_n$ is the $n$-th row vector of the $\mathbf{D}$ matrix containing the normal vibrational modes in internal coordinates $\mathbf{q}$ [91–93].

$$\mathbf{d}_n = \mathbf{b}_n\mathbf{L}, \tag{2}$$

where matrix L contains $3N$ mode vectors, and matrix B is the rectangular matrix of the internal coordinate first derivatives. Eq. (1) reveals that only matrices $\mathbf{K}$ and $\mathbf{D}$ are needed to determine $\mathbf{a}_n$, i.e. once the normal mode analysis is completed, subsequent local mode analysis is straight forward [89,90].

To each local mode $\mathbf{a}_n$ local properties can be assigned. The local mode force constant $k_n^a$ of mode $n$ (superscript $a$ denotes an adiabatically relaxed, i.e. local mode) is obtained via Eq. (3):

$$k_n^a = \mathbf{a}_n^\dagger \mathbf{K} \mathbf{a}_n = \left(\mathbf{d}_n \mathbf{K}^{-1} \mathbf{d}_n^\dagger\right)^{-1} \qquad (3)$$

In recent work, Zou and co-workers proved that the compliance constants $\Gamma_{nn}$ of Decius [94] are simply the reciprocal of the local mode force constants: $k_n^a = 1/\Gamma_{nn}$ [87].

The local mode mass $m_n^a$ of mode $n$ is given by

$$m_n^a = 1/G_{n,n} = \left(\mathbf{b}_n \mathbf{M}^{-1} \mathbf{b}_n^\dagger\right)^{-1} \qquad (4)$$

where $G_{n,n}$ is the $n$-th diagonal element of the Wilson $\mathbf{G}$, and $\mathbf{M}$ is the mass matrix [91,92]. The local mode force constant and mass are needed to determine the *local mode frequency* $\omega_n^a$

$$\left(\omega_n^a\right)^2 = \frac{1}{4\pi^2 c^2} k_n^a G_{nn} \qquad (5)$$

Apart from these properties, it is straightforward to determine the local mode infrared intensity [95]. As shown by Konkoli and Cremer [96,97] the normal vibrational modes can be decomposed into local mode components for a complete, non-redundant set of $N_{\text{vib}}$ local modes, leading to the detailed analysis of a vibrational spectrum and in this way decoding a wealth of information hidden in the vibrational spectrum [98,99]. Konkoli and Cremer [96,97] introduced the amplitude $A$ which provides a measure for the contribution of the local vibrational modes to each normal vibrational mode. For this purpose they defined $A$ as a function of normal mode $\mathbf{I}_\mu$ and local mode $\mathbf{a}_n$

$$A_{n\mu} = f\left(\mathbf{I}_\mu, \mathbf{a}_n\right) \qquad (6)$$

with

$$A_{n\mu} = \frac{\left(\mathbf{I}_\mu, \mathbf{a}_n\right)^2}{\left(\mathbf{a}_n, \mathbf{a}_n\right)\left(\mathbf{I}_\mu, \mathbf{I}_\mu\right)} \qquad (7)$$

The denominator in Eq. (7) normalizes $A$ so that its value lies between 0 and 1. The matrix $(\mathbf{a},\mathbf{b})$ in Eq. (7) is expressed as

$$(\mathbf{a}, \mathbf{b}) = \sum_{i,j} a_i f_{ij} b_j \qquad (8)$$

where $a \in [\mathbf{I}_\mu, \mathbf{a}_n]$, $b \in [\mathbf{I}_\mu, \mathbf{a}_n]$ and $f_{ij}$ is an element of the force constant matrix $\mathbf{F}^x$ expressed in Cartesian coordinates. Once $A$ is defined, the percentage of the local mode contributions to a certain normal mode can be compared using the following:

$$A_{n\mu}^\% = \frac{A_{n\mu}}{\sum_m A_{m\mu}} 100 \qquad (9)$$

where $\sum_m A_{m\mu}$ represents the sum of all amplitudes related to the normal mode in question.

The local mode analysis has successfully characterized covalent bonds [88,100–105] in addition to weak chemical interactions such as halogen [106–108], chalcogen [109–111], pnicogen [112–114], and tetrel bonds [115], as well as including H-bonding [98,116–118]. Local vibrational force constants could also clearly illustrate that a shorter bond is not always a stronger bond [90,96,97,102], and recently the local mode analysis was extended to periodic systems and crystals [119]. The local mode analysis and the characterization of normal modes study was performed with COLOGNE2019 [120]. In order to determine the covalent versus electrostatic character in weakly bonded donor-acceptor complexes, the energy density $H(\mathbf{r})$ originally introduced by Cremer and Kraka [118,121] was applied. A covalent interaction has a stabilizing negative $H(\mathbf{r}_c) = H_c$ value at the bond critical

point $\mathbf{r}_c(AB)$ of the electronic density distribution $\rho(\mathbf{r})$ between atoms A and B forming the bonding in question. Noncovalent interactions (electrostatic or of dispersion type) are characterized by positive or close to zero value of $H_c$ [118,121]. The electron density analysis was performed with the AIMAll program [122].

### 2.3. Spectroscopic constants

PECs were obtained by performing several single-point CCSD(T)/ aVTZ calculations (fixed optimized geometries of the dimer) and varying the distance between monomers at the optimized geometry. The PEC was fitted using the following extended Rydberg analytical form [123]:

$$V(R) = -D_e \left[1 + \sum_{k=1}^{N=10} c_k (R-R_e)^k\right] e^{-c_1(R-R_e)}, \qquad (10)$$

where $D_e$ is the dissociation energy, $R_e$ is the equilibrium distance, and $c_k$ are the coefficients that will be determined. Said parameters were determined through the Powell method [124]. The rovibrational spectroscopic constants were obtained using the Dunham method [125] given by the following expressions [9,75,76]:

$$\omega_e = \frac{1}{24}\left[141\left(\varepsilon_{1,0}-\varepsilon_{0,0}\right)-93\left(\varepsilon_{2,0}-\varepsilon_{0,0}\right)+23\left(\varepsilon_{3,0}-\varepsilon_{1,0}\right)\right] \qquad (11)$$

$$\omega_e x_e = \frac{1}{4}\left[13\left(\varepsilon_{1,0}-\varepsilon_{0,0}\right)-11\left(\varepsilon_{2,0}-\varepsilon_{0,0}\right)+3\left(\varepsilon_{3,0}-\varepsilon_{1,0}\right)\right] \qquad (12)$$

$$\omega_e y_e = \frac{1}{6}\left[3\left(\varepsilon_{1,0}-\varepsilon_{0,0}\right)-3\left(\varepsilon_{2,0}-\varepsilon_{0,0}\right)+\left(\varepsilon_{3,0}-\varepsilon_{1,0}\right)\right] \qquad (13)$$

$$\alpha_e = \frac{1}{8}\left[-12\left(\varepsilon_{1,1}-\varepsilon_{0,1}\right)+4\left(\varepsilon_{2,1}-\varepsilon_{0,1}\right)+4\omega_e-23\omega_e y_e\right] \qquad (14)$$

$$\gamma_e = \frac{1}{4}\left[-2\left(\varepsilon_{1,1}-\varepsilon_{0,1}\right)+\left(\varepsilon_{2,1}-\varepsilon_{0,1}\right)+2\omega_e x_e-9\omega_e y_e\right], \qquad (15)$$

where $\varepsilon_{v,j}$ represents the rovibrational energies which were obtained by solving the nuclear Schrodinger equation with the discrete variable method (DVR) [126–128].

Slater presents theory for the polyatomic unimolecular gas reaction based on models from the vibrations of the molecule with the quadratic potential function [129]. From this theory it is possible to calculate the unimolecular decomposition of the complex accounting for electronic dissociation energy, $D_e$. In this case, when the frequency of decomposition is correlated to the vibration, where the rate constant is in term of this frequency given by [129,130]

$$k(T) = \omega_e e^{-\frac{D_e - \varepsilon_{0,0}}{RT}}. \qquad (16)$$

The decomposition lifetime is the reciprocal of the rate constant. This method was recently applied for the analysis of van der Waals complexes [74] and is determined by [129,130]

$$\tau(T) = \frac{1}{k(T)} e^{\frac{D_e - \varepsilon_{0,0}}{RT}}. \qquad (17)$$

## 3. Results and discussion

### 3.1. Local vibrational mode analysis

Fig. 1 depicts the structure of hydrogen sulfide dimer. The equilibrium geometry of the dimer is similar to that of water dimer of $C_s$ symmetry [23–25]. The donor bond S1-H3 is directed toward S4 of acceptor
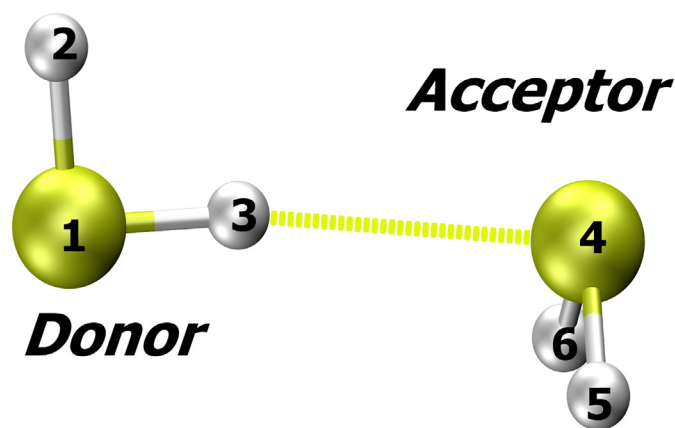
**Fig. 1.** Optimized structure of $H_2S$ dimer showing the notation used for the atoms throughout the text. H-bond donor left side, H-bond acceptor right side. Yellow for sulfur and white for hydrogen.

(Table S1 of Supplementary information), and this is one important distance for the local vibrational mode analysis.

Table 1 presents the optimized geometry results. The distance between the two monomers, H3⋯S4, is in the range of 2.743 and 2.801 Å, in accordance with an experimental microwave spectroscopy value of 2.778(9) Å [27], and high level theoretical values of 2.830 Å at CCSD(T)/ha(Q + d)Z [22], and of 2.787 Å using MP2-CP/aV(Q + d)Z [73]. The largest deviation from the experimental interatomic distance is <1.3% for MP2/aVTZ. CCSD(T)/aVDZ and CCSD(T)/aVTZ with 2.795 and 2.801 Å give errors of 0.8 and 0.6% in the relation to the experimental value, respectively. It is interesting to note that this distance is larger (2.743–2.801 Å) than the analogous interaction in water dimer of almost 2.020 Å [23].

The d(S1⋯S4) interatomic distance is also in reasonable agreement with the experimental value of 4.112(1) Å. CCSD(T)/aVDZ and CCSD(T)/aVTZ S1⋯S4 distances are 4.147 and 4.138 Å giving errors of 0.3 and 0.5%, respectively. Dreux and Tschumper calculated a distance of 4.16 Å at the CCSD(T)/ha(Q + d)Z level of theory [22]. Lemke reported a value of 4.146 Å using CCSD(T)/aVQZ [21], while the equilibrium geometry at CP corrected potential energy surface was 4.178 Å [21]. The S⋯S interatomic distance of 4.112 Å is larger than the related 2.977 Å O⋯O distance of water dimer [23], which is correlated to the weaker interaction found for $H_2S$ dimer. We also report the equilibrium distance of the center of mass that will be used for the local force constant analysis. The theoretical result of 4.106 Å reported for the MP2 level [26] is close to our results. The average calculated S-H⋯S angle connecting monomers is 173.4°, a 0.9% error compared to the experimental angle of 175.0° [27]. Moreover, the literature value for the aforementioned angle was previously calculated as 171.0° at the CCSD(T)/ha(Q + d)Z level of theory [22].

Table 2 shows the $H_2S$ dimer computed energies. The experimental binding energy is 7.06 kJ mol$^{-1}$ [65]. CCSD(T)/ha(Q + d)Z [22] was

**Table 1**
Interatomic distances (Å) and bond angles (°).

|  | H3⋯S4 | S1⋯S4[a] | R(A⋯B) | S1-H3⋯S4 |
|---|---|---|---|---|
| MP2/aVDZ | 2.750 | 4.097 | 3.897 | 173.2 |
| MP2/aVTZ | 2.743 | 4.076 | 3.855 | 172.7 |
| MP2/aVQZ | 2.752 | 4.080 | 3.863 | 171.8 |
| CCSD(T)/aVDZ | 2.795 | 4.147 | 3.942 | 173.5 |
| CCSD(T)/aVTZ | 2.801 | 4.138 | 3.911 | 172.2 |
| Experiment [27] | 2.778 | 4.112 | – | 175.0 |

(A⋯B) stands for the center-of-mass interatomic distance. H-S-H$_d$ is the donor angle A(3−1−2).

[a] The S1⋯S4 distance values were also reported by Lemke [21].

**Table 2**
Energies for the $H_2S$ dimer in kJ mol$^{-1}$. Thermodynamic quantities are given at 298.15 K. ZPE using harmonic frequencies.

|  | $D_e$ | $D_{e,cp}$ | ΔH | ΔG | $D_{e,cp}$ + ZPE |
|---|---|---|---|---|---|
| MP2/aVDZ | 9.87 | 6.49 | −4.20 | 18.37 | 1.68 |
| MP2/aVTZ | 8.91 | 7.32 | −3.38 | 17.11 | 3.04 |
| MP2/aVQZ | 8.45 | 7.70 | −2.96 | 17.03 | 3.55 |
| CCSD(T)/aVDZ | 9.04 | 7.17 | −3.56 | 14.93 | 2.55 |
| CCSD(T)/aVTZ | 7.90 | 7.05 | −2.58 | 16.81 | 3.01 |

reported with the $D_e$ of 6.65 kJ mol$^{-1}$ (with CP), while CCSD(T)/aVQZ [21] showed the value for $D_e$ of 7.38 kJ mol$^{-1}$ and including CP of 6.87 kJ mol$^{-1}$. Therefore, our calculated $D_e$ with CP and including ZPE are supported by experimental and theoretical data. CCSD(T)/aVTZ calculations have the smallest error of 0.1% for $D_e$ (7.05 kJ mol$^{-1}$). $D_e$ including ZPE values shows the same trend found in the literature, being 3.01 kJ mol$^{-1}$ for the CCSD(T)/aVTZ. The binding energy (corrected with CP and ZPE) reported for optimized geometry at MP2/aug-cc-pVTZ is 3.39 kJ mol$^{-1}$, while the $D_e$ is 7.32 kJ mol$^{-1}$ [28]. CCSD(T)/ha (Q + d)Z [22] was reported with the $D_e$ of 6.65 kJ mol$^{-1}$ (with CP), while including ZPE was 3.34 kJ mol$^{-1}$ [22]. Enthalpy of formation for the dimer is −2.58 kJ mol$^{-1}$ at CCSD(T)/aVTZ, while the Gibbs free energy is 16.81 kJ mol$^{-1}$, compared to the values of −2.30 and 12.80 kJ mol$^{-1}$ at CCSD(T)/ha(Q + d)Z [22].

The harmonic normal mode frequencies calculated via analytical second derivatives are shown in Table 3, while the Konkoli-Cremer local mode frequencies and local force constants are shown in Supplementary information (Tables S2 and S3). Fig. 2 shows the normal mode decomposition into local mode contributions from the CCSD(T)/aVTZ level of theory. The experimental S—H ($\nu_{S-H}^b$) mode of H-bond donating is assigned to the frequency of 2590 cm$^{-1}$ [28,32]. Our result of normal mode frequency at CCSD(T)/aVTZ is 2686 cm$^{-1}$ with an intensity of 51.237 km/mol, while the CCSD(T)/aVDZ value is 2673 cm$^{-1}$ and has an intensity of 35.296 km/mol. Anharmonic computation from second-order vibrational perturbation theory (VPT2) corrects this frequency to 2606 cm$^{-1}$ at CCSD(T)/ha(Q + d)Z [22]. This mode was assigned by the local vibrational mode analysis to the S1-H3 of the H-bond donating $H_2S$ in accordance to the theoretical and experimental results of the literature [21,22,28,32]. This $\nu_{S-H}^b$ normal mode frequency corresponds to a redshift of 33 cm$^{-1}$ for CCSD(T)/aVTZ (30 cm$^{-1}$ for the CCSD(T)/aVDZ), in accordance with the experimental 31 cm$^{-1}$ in relation to the central frequency of $\nu_1$ and $\nu_3$ of

**Table 3**
Harmonic $\omega$ (cm$^{-1}$) and anharmonic $\nu$ (cm$^{-1}$) vibrational frequencies. The last column is the shift of lowest frequency (cm$^{-1}$) regarding the mean value of calculated monomer frequencies.

|  | $\omega_1$ | $\omega_2$ | $\omega_3$ | $\omega_4$ |  |
|---|---|---|---|---|---|
| **Harmonic** |  |  |  |  |  |
| MP2/aVDZ [28] | 2719 | 2750 | 2769 | 2775 | −49 |
| MP2/aVTZ [28,32] | 2730 | 2769 | 2784 | 2789 | −57 |
| MP2/aVQZ [21] | 2731 | 2771 | 2786 | 2791 | −54 |
| CCSD(T)/aVDZ | 2673 | 2689 | 2706 | 2710 | −30 |
| CCSD(T)/aVTZ | 2686 | 2708 | 2720 | 2725 | −33 |
| CCSD(T)/aVQZ [21] | 2691 | 2714 | 2726 | 2729 | −34 |
|  |  |  |  |  |  |
| **Anharmonic** |  |  |  |  |  |
| MP2/aVDZ | 2634 | 2652 | 2670 | 2674 | −36 |
| MP2/aVTZ | 2651 | 2671 | 2684 | 2688 | −34 |
| MP2/aVQZ | 2654 | 2674 | 2688 | 2691 | −34 |
| CCSD(T)/aVDZ[a] | 2588 | 2591 | 2607 | 2610 | −16 |
| CCSD(T)/aVTZ[a] | 2607 | 2610 | 2621 | 2623 | −10 |
| CCSD(T)/aVQZ [21][a] | 2615 | 2615 | 2627 | 2629 | −13 |
| Experiment [28] | $\nu_{S-H}^b$ | $\nu_1^a$ | $\nu_{S-H}^f$ | $\nu_3^a$ |  |
| Gas phase | 2590 | 2605 | 2618 | 2618 | −31 |

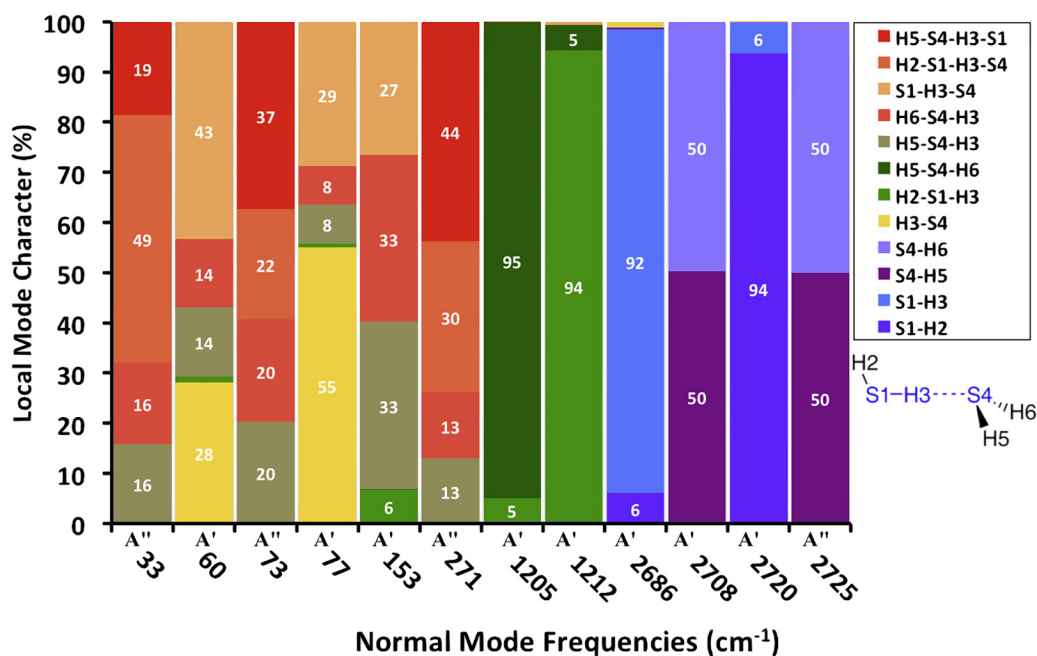[a] $\nu_i[CCSD(T) / aVXZ] = \omega_i[CCSD(T) / aVXZ] + \nu_i[MP2 / aVXZ] - \omega_i[MP2 / aVXZ]$.

**Fig. 2.** Decomposition of CCSD(T)/aVTZ normal modes into local mode contributions, given in %. The normal modes with their irreducible representations are given as a bar diagram, and the local modes are color-coded according to the legend.

H₂S [28]. The S1-H3 bond distance is the largest of the SH group distances (Table S1), which is in accordance with the H-bond formation, and with the lowest local force constant of 4.151 mdyn/Å at CCSD(T)/aVTZ.

VPT2 anharmonic correction (Table 3) for the frequency shift shows better agreement at MP2 level, while the harmonic frequencies overestimate this shift. The reverse was found for the CCSD(T) using the composite method [22] combining the MP2 anharmonic correction, where the harmonic frequencies are in better agreement to the shift value than the anharmonic. It is interesting to note that the shift value (in relation to the monomer frequencies) is almost the same as the difference between the two frequencies associated to the donor modes, $\nu_{S-H}^b$ and ($\nu_{S-H}^f$). This trend will also support the assignment of 2618 cm$^{-1}$ vibrational frequency to the free donor S—H bond.

The experimental value of second vibrational mode is at 2605 cm$^{-1}$ and corresponds to the symmetric S—H stretch of the acceptor H₂S moiety ($\nu_1^a$) [28]. The local vibrational mode analysis assigned this frequency to the S4-H5 and S4-H6 bonds of the acceptor moiety, which is in agreement with experimental and theoretical literature values [22,28,32]. This mode has the intensity of 0.144 km/mol, much smaller than the $\nu_{S-H}^b$ mode, in accordance to experimental data reported that the intensity of $\nu_{S-H}^b$ mode is 10 times greater than the $\nu_1^a$. The anharmonic correction at CCSD(T)/ha(Q + d)Z of Dreux and Tschumper leads to the value of 2610 cm$^{-1}$ [22]. It was shown by Cremer and Kraka that local mode analysis is based on normal mode frequencies, then the calculated frequencies do not require anharmonic corrections [86].

According to experiment, the last two modes are $\nu_3$ signatures at 2618 cm$^{-1}$ [28] or at 2622 cm$^{-1}$ with intensity of 10 km/mol [32]; the authors however could not attribute these modes to the proton donor or acceptor [32]. The local vibrational mode analysis is able to resolve this vibration, and assigned the mode at 2720 cm$^{-1}$ for the free S1-H2 ($\nu_{S-H}^f$) of the donor moiety. This trend is in agreement with observations of water dimer [116]. Complementary to the H-bonding, the force constant associated to the S1-H2 ($\nu_{S-H}^f$) of 4.245 mdyn/Å at CCSD(T)/aVTZ is the largest force constant compared to the SH group force constants. In general, these force constants are smaller than the same found for the water molecule, of 7.641 mdyn/Å [116]. It is also remarkable that the force constants show the same trend independent of

method and basis set used. The vibrational mode at 2725 cm$^{-1}$ is the same found for the 2708 cm$^{-1}$, the stretching of S4-H5 and S4-H6 bonds of the acceptor moiety of H₂S.

Lemke [21] showed a CCSD/aVQZ harmonic frequency of 261 cm$^{-1}$ and an extrapolated anharmonic of 197 cm$^{-1}$. The local mode assignment for the harmonic normal mode of CCSD/aVTZ at 271 cm$^{-1}$ is for the H2-S1-H3-S4 and H5-S4-H3-S1 torsions connected to the out of plane bending of acceptor. The CCSD/aVTZ at 153 cm$^{-1}$ through the local mode is related to the acceptor wag. The most important of this group is the CCSD/aVTZ at 77 cm$^{-1}$, which is related to the hydrogen bond stretching and has contribution of the donor bending. The local mode analysis suggests that local mode S1-H3 stretching dominates $\nu_{S-H}^b$, the S4-H5 and S4-H6 local mode stretchings $\nu_1^a$, the local mode S1-H2 stretching $\nu_{S-H}^f$ and the local mode S4-H5 and S4-H6 stretching $\nu_3^a$, providing a comprehensive analysis of these normal vibrational modes.

The H₂S molecule shows a $\nu_2$ mode observed at 1183 cm$^{-1}$ corresponding to the H-S-H bending [53,62]. Our calculated vibrational mode of the H₂S free molecule is at 1206 cm$^{-1}$ for the CCSD(T)/aVTZ level, while the dimer shows a shift to 1205 and 1212 cm$^{-1}$. The local modes have assigned to the acceptor (H5-S4-H6) and donor (H2-S1-H3) bending modes, respectively. These results are close to the experimental values of 1179 and 1183 cm$^{-1}$ for the H₂S dimer [32]. The CCSD(T)/aVQZ harmonic frequencies was reported at 1207 cm$^{-1}$ (acceptor) and 1213 cm$^{-1}$ (donor), while the anharmonic modes were reported at 1180 cm$^{-1}$ (acceptor) and 1182 cm$^{-1}$ (donor) [21]. This assignment is in the same order found for water dimer, for the local and normal modes, both theoretical and experimental results [116]. This feature is explained by the local mode decomposition analysis, where the main contribution to the 1205 cm$^{-1}$ is from the local mode of acceptor H-S-H bending, with a small contribution of donor bending. Otherwise, the 1212 cm$^{-1}$ from the local mode is mainly from the donor bending with a small contribution of acceptor bending. The agreement in the band shifts compared to experiment data has to be treated cautiously, as the simple treatment of the nuclear motion was used, while the weakly bound hydrogen sulfide dimer goes complicated nuclear motion.

Table 4 shows the local vibrational mode analysis for the H···S bond and density properties of the H₂S dimer. Local stretching force constants obtained with the harmonic approximation are expected to provide a

**Table 4**
Properties of local modes analysis and energy density distribution associated to H⋯S bonding in the $H_2S$ dimer.[*]

|  | $k^a$ (A⋯B) | $\omega^a$ | $k^a$ (H3⋯S4) | $\omega^a$ | $\rho$ (e/Å³) | $H_c$ (h/Å³) | $H_c/\rho$ (h/e) |
|---|---|---|---|---|---|---|---|
| MP2/aVDZ | 0.029 | 148 | 0.057 | 316 | 0.071 | 0.003 | 0.036 |
| MP2/aVTZ | 0.024 | 134 | 0.052 | 301 | 0.072 | 0.005 | 0.063 |
| MP2/aVQZ | 0.022 | 131 | 0.049 | 293 | 0.071 | 0.004 | 0.051 |
| CCSD(T)/aVDZ | 0.027 | 142 | 0.054 | 305 | 0.064 | 0.003 | 0.053 |
| CCSD(T)/aVTZ | 0.021 | 125 | 0.046 | 283 | 0.063 | 0.006 | 0.098 |

[*] Local mode force constants $k^a$ in mdyn/Å, frequency $\omega^a$ in cm⁻¹, electron density $\rho_c$ at the bond critical point in e/Å³, energy density $H_c$ at the bond critical point in Hartree/Å³, and energy density per electron $H_c/\rho$ in Hartree. $k^a$(A⋯B) is relative to the center-of-mass of the two monomers.

reliable descriptor of the relative H-bond strength [86]. Despite the large range of interatomic distances regarding the center-of-mass of each $H_2S$ molecule (Table S1) between 3.8552 Å (MP2/aVTZ) and 3.9424 Å (CCSD (T)/aVDZ), the related $k^a$(A⋯B) shows closer force constant values associated with the interaction between these two monomers. Furthermore, the force constant of H3⋯S4 (H-bonding) is almost twice the A⋯B value, and H3⋯S4 force constant is smaller than the 0.085 mdyn/Å of water [116]. The smallest force constants and frequencies are in accordance with the weak interaction of the $H_2S$ dimer. As shown in Table 4 the H⋯S bond is characterized by a small positive $H_c$ value independent on the model chemistry used, while the H⋯O hydrogen bond in the water dimer has a negative value (−0.005 h/Å³) [118,121]. The positive sign of $H_c$ for H⋯S suggests a noncovalent interaction. In contrast, the negative sign of $H_c$ identifies the hydrogen bonding in the water dimer as covalent.

### 3.2. Rovibrational constants

The experimental value for the (B + C) / 2 rotational constant for the $H_2S$ dimer was determined as 0.05834 cm⁻¹ [27], and has been studied using MP2 with a several basis sets and found values between 0.054844 and 0.057940 cm⁻¹ [26], while the theoretical MP2/aVDZ shows a value of 0.059052 cm⁻¹ (1770.3 MHz) [27]. Based on microwave spectroscopy, the fitting of rotational constants gives B = 0.058477 cm⁻¹ (1752.9 MHz) and C = 0.058144 cm⁻¹ (1745.7 MHz) for the lower state, and B = 0.058470 cm⁻¹, C = 0.058232 cm⁻¹ for the upper state [27]. Our calculated CCSD(T)/aVTZ B and C rotational constants are close to the experimental data, being 0.058130 cm⁻¹ and 0.057840 cm⁻¹, respectively. The calculated A rotational constant value at CCSD(T)/aVTZ is 3.20743 cm⁻¹ (96,156.4 MHz).

Full determination of internal quantum states is required to any property calculation at low temperature, where the $H_2S$ dimer populates exclusively low lying levels. Consequently, we must also properly take into account all degree of freedom of the interacting $H_2S$ dimer, including vibration and bending of each non frozen monomer. Nevertheless, origin and meaning of the PEC exploited in this study indicates that it can be used to assess these properties at sufficiently high temperatures. Under these circumstances, the intermolecular stretching could play the principal role, while the other degrees of freedom of monomer (mostly the bending modes) contribute as statistical averages over all accessible $H_2S$ orientations internally to each monomer.

From the solution of the nuclear Schrödinger equation using the DVR method and the calculated CCSD(T)/aVTZ PEC described by Eq. (10), we found eighteen vibrational levels for the H2S⋯H2S system. The structure was treated as a pseudo-diatomic molecule in which both monomers are essentially spherical. To calculate the system rovibrational energies a total of 500 Gaussian quadratures were used and only those energies smaller than the dissociation energies of the system are described in their respective potential energy curves. Table 5 presents the $H_2S$ dimer rovibrational constants determined by both methods of Dunham

**Table 5**
Rovibrational spectroscopic constants (cm⁻¹).

|  | DVR | Dunham |
|---|---|---|
| $\omega_e$ | 68.4561 | 68.4350 |
| $\omega_e x_e$ | 2.01936 | 2.00714 |
| $\omega_e y_e$ | $1.89517 \times 10^{-3}$ | $2.26089 \times 10^{-3}$ |
| $\alpha_e$ | $1.40216 \times 10^{-3}$ | $1.40529 \times 10^{-3}$ |
| $\gamma_e$ | $2.89517 \times 10^{-5}$ | $2.67738 \times 10^{-5}$ |

and Eqs. (11)–(15). Rovibrational energies and the coefficient for the CEP of order 10 are in Supplementary information (Table S4). The complex has a (B + C) / 2 rotational constant from Dunham of 0.057785 cm⁻¹, which is close to the experimental value [27]. The harmonic vibrational constant of almost 68 cm⁻¹ using Dunham or DVR methods shows the weak stability of this complex. The obtained dissociation energy was used to calculate the lifetime of the decomposition of the complex (Fig. 3) as a function of temperature (from 200 to 500 K). The lifetime shows a value higher than 1 ps for the complete temperature interval. Therefore, following the Slater theory [129,130], the complex is considered stable.

## 4. Conclusions

In this work, we investigated the intrinsic hydrogen bond strength of $H_2S$ dimer using the MP2/aug-cc-pV(D,T,Q)Z and the CCSD(T)/aug-cc-pV(D,T)Z. The local vibrational mode analysis achieved a resolution for the free S—H vibration ($\nu^f_{S-H}$) of the donor moiety. These results provide an outline for the main question of the literature about the vibrational mode assigned to the bond stretching of $H_2S$ donor and acceptor. The $H_2S$ dimer local force constants were compared to the water dimer of the literature. It was verified from this comparison that the local force constant of hydrogen bonding in the hydrogen sulfide dimer is smaller than the value for the water dimer. The smaller force constants are in accordance with the weaker hydrogen bonding in the $H_2S$ dimer. Furthermore, the lowest energy vibrational $v_2$ modes were also assigned by the local modes to the donor and acceptor bending modes. The rotational constants are supported by the experimental results of the literature. The potential energy curve rotational constant is also close to the experimental value, and the lifetime for the complex decomposition shows a stable dimer.
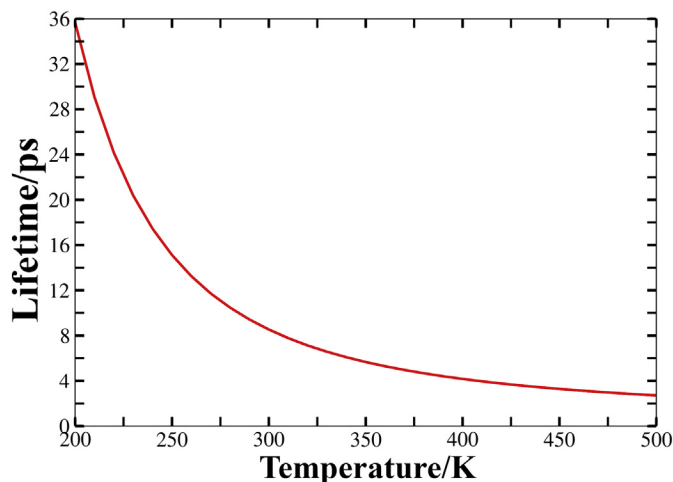


**Fig. 3.** Lifetime (ps) for the complex decomposition.

## CRediT authorship contribution statement

**João B.L. Martins:** Supervision, Writing - review & editing. **Rabeshe P. Quintino:** Investigation, Formal analysis. **José R. dos S. Politi:** Investigation, Formal analysis. **Daniel Sethio:** Investigation, Formal analysis. **Ricardo Gargano:** Investigation, Formal analysis. **Elfi Kraka:** Investigation, Formal analysis.

## Declaration of competing interest

The authors declare that they have no known competing financial interests or personal relationships that could have appeared to influence the work reported in this paper.

## Acknowledgments

## Appendix A. Supplementary data

Supplementary data to this article can be found online at https://doi.org/10.1016/j.saa.2020.118540.

## References

[1] M. Rezaei, N. Moazzen-Ahmadi, A.R.W. McKellar, B. Fernandez, D. Farrelly, Towards an understanding of the helium-acetylene van der Waals complex, Mol. Phys. 110 (2012) 2743–2750, https://doi.org/10.1080/00268976.2012.699108.

[2] N. Moazzen-Ahmadi, A.R.W. McKellar, Spectroscopy of dimers, trimers and larger clusters of linear molecules, Int. Rev. Phys. Chem. 32 (2013) 611–650, https://doi.org/10.1080/0144235X.2013.813799.

[3] E.A. Orabi, A.M. English, Sulfur-aromatic interactions: modeling cysteine and methionine binding to tyrosinate and histidinium ions to assess their influence on protein electron transfer, Israel J. Chem. 56 (2016) 872–885, https://doi.org/10.1002/ijch.201600047.

[4] I.C. Gerber, J.G. Ángyán, London dispersion forces by range-separated hybrid density functional with second order perturbational corrections: the case of rare gas complexes, J. Chem. Phys. 126 (2007) 44103, https://doi.org/10.1063/1.2431644.

[5] J. Hermann, R.A. DiStasio, A. Tkatchenko, First-principles models for van der Waals interactions in molecules and materials: concepts, theory, and applications, Chem. Rev. 117 (2017) 4714–4758, https://doi.org/10.1021/acs.chemrev.6b00446.

[6] H.S. Biswal, S. Bhattacharyya, A. Bhattacherjee, S. Wategaonkar, Nature and strength of sulfur-centred hydrogen bonds: laser spectroscopic investigations in the gas phase and quantum-chemical calculations, Int. Rev. Phys. Chem. 34 (2015) 99–160, https://doi.org/10.1080/0144235X.2015.1022946.

[7] C.R. Forbes, S.K. Sinha, H.K. Ganguly, S. Bai, G.P.A. Yap, S. Patel, N.J. Zondlo, Insights into thiol-aromatic interactions: a stereoelectronic basis for S-H/pi interactions, J. Am. Chem. Soc. 139 (2017) 1842–1855, https://doi.org/10.1021/jacs.6b08415.

[8] J.B.L. Martins, J.R.S. Politi, E. Garcia, A.F.A. Vilela, R. Gargano, Theoretical study of CH4-CH4, CHF3-CH 4, CH4-H2O, and CHF3-H2O dimers, J. Phys. Chem. A 113 (2009) 14818–14823, https://doi.org/10.1021/jp904962b.

[9] W.F. Cunha, R. Gargano, E. Garcia, J.R.S. Politi, A.F. Albernaz, J.B.L. Martins, Rovibrational energy and spectroscopic constant calculations of CH4 center dot center dot center dot CH4, CH4 center dot center dot center dot H2O, CH4 center dot center dot center dot CHF3, and H2O center dot center dot center dot CHF3 dimers, J. Mol. Model. 20 (2014) 2298, https://doi.org/10.1007/s00894-014-2298-1.

[10] W.F. da Cunha, R.M. de Oliveira, L.F. Roncaratti, J.B.L. Martins, G.M. e Silva, R. Gargano, Rovibrational energies and spectroscopic constants for H2O-Ng complexes, J. Mol. Model. 20 (2014) 2–7, https://doi.org/10.1007/s00894-014-2498-8.

[11] J.B.L. Martins, J.R.D. Politi, A.D. Braga, R. Gargano, Complexes of water with the fluoromethanes, Chem. Phys. Lett. 431 (2006) 51–55, https://doi.org/10.1016/j.cplett.2006.09.065.

[12] T.C. Preston, R. Signorell, Infrared spectroscopy and modeling of co-crystalline CO2 center dot C2H2 aerosol particles. II. The structure and shape of co-crystalline CO2 center dot C2H2 aerosol particles, J. Chem. Phys. 136 (2012) 094510, https://doi.org/10.1063/1.3690064.

[13] S.L. Stephens, W. Mizukami, D.P. Tew, N.R. Walker, A.C. Legon, Distortion of ethyne on formation of a pi complex with silver chloride: C2H2 center dot center dot center dot Ag-Cl characterised by rotational spectroscopy and ab initio calculations, J. Chem. Phys. 137 (2012) 174302, https://doi.org/10.1063/1.4761895.

[14] K. Shuler, C.E. Dykstra, Interaction potentials and vibrational effects in the acetylene dimer, J. Phys. Chem. A 104 (2000) 4562–4570, https://doi.org/10.1021/jp9940405.

[15] V.I. Makarov, S.A. Kochubei, I. Khmelinskii, Photodissociation of (SO2 center dot center dot center dot XH) Van der Waals complexes and clusters (XH = C2H2, C2H4, C2H6) excited at 32 040–32 090 cm(−1) with formation of HSO2 and X, J. Chem. Phys. 140 (2014), 054304, https://doi.org/10.1063/1.4863445.

[16] C. Lauzin, L.H. Coudert, M. Herman, J. Lievin, Ab Initio intermolecular potential of Ar-C2H2 refined using high-resolution spectroscopic data, J. Phys. Chem. A 117 (2013) 13767–13774, https://doi.org/10.1021/jp408013n.

[17] S.-Y. Li, D. Wu, Y. Li, D. Yu, J.-Y. Liu, Z.-R. Li, Insight into structural and pi-magnesium bonding characteristics of the X2Mg center dot center dot center dot Y (X = H, F; Y = C2H2, C2H4 and C6H6) complexes, RSC Adv. 6 (2016) 102754–102761, https://doi.org/10.1039/c6ra23368f.

[18] L.C. Carvalho, M.A. Bueno, B.G. de Oliveira, The interplay and strength of the π···HF, C···HF, F···HF and F···HC hydrogen bonds upon the formation of multimolecular complexes based on C2H2···HF and C2H4···HF small dimers, Spectrochim. Acta A 213 (2019) 438–455, https://doi.org/10.1016/j.saa.2019.01.004.

[19] C. Tantardini, When does a hydrogen bond become a van der Waals interaction? A topological answer, J. Comput. Chem. 40 (2019) 937–943, https://doi.org/10.1002/jcc.25774.

[20] S. Tsuzuki, A. Fujii, Nature and physical origin of CH/π interaction: significant difference from conventional hydrogen bonds, Phys. Chem. Chem. Phys. 10 (2008) 2584–2594, https://doi.org/10.1039/B718656H.

[21] K.H. Lemke, Structure and binding energy of the H2S dimer at the CCSD (T) complete basis set limit, J. Chem. Phys. 146 (2017) 234301, https://doi.org/10.1063/1.4985094.

[22] K.M. Dreux, G.S. Tschumper, Examination of the structures, energetics, and vibrational frequencies of small sulfur-containing prototypical dimers, (H2S) 2 and H2O/H2S, J. Comput. Chem. 40 (2019) 229–236, https://doi.org/10.1002/jcc.25578.

[23] J.A. Odutola, T.R. Dyke, Partially deuterated water dimers: microwave spectra and structure, J. Chem. Phys. 72 (1980) 5062–5070, https://doi.org/10.1063/1.439795.

[24] A. Mukhopadhyay, W.T.S. Cole, R.J. Saykally, The water dimer I: experimental characterization, Chem. Phys. Lett. 633 (2015) 13–26, https://doi.org/10.1016/j.cplett.2015.04.016.

[25] A. Mukhopadhyay, S.S. Xantheas, R.J. Saykally, The water dimer II: theoretical investigations, Chem. Phys. Lett. 700 (2018) 163–175, https://doi.org/10.1016/j.cplett.2018.03.057.

[26] G. de Oiveira, C.E. Dykstra, Large basis-set study of the stability of (h2s)(2) - the importance of 3d functions in weak interaction of 2nd row molecules, Chem. Phys. Lett. 243 (1995) 158–164, https://doi.org/10.1016/0009-2614(95)00792-3.

[27] A. Das, P.K. Mandal, F.J. Lovas, C. Medcraft, N.R. Walker, E. Arunan, The H2S dimer is hydrogen-bonded: direct confirmation from microwave spectroscopy, Angew. Chemie - Int. Ed. (2018)https://doi.org/10.1002/anie.201808162.

[28] A. Bhattacherjee, Y. Matsuda, A. Fujii, S. Wategaonkar, The intermolecular S-H···Y (Y=S,O) hydrogen bond in the H2S dimer and the H2S-MeOH complex, ChemPhysChem. 14 (2013) 905–914, https://doi.org/10.1002/cphc.201201012.

[29] D.E. Woon, D.R. Beck, Ab initio potentials for (H2S)2, including studies of effects from third-order many-body perturbation theory and three-body nonadditivity, J. Chem. Phys. 92 (1990) 3605–3609, https://doi.org/10.1063/1.457868.

[30] G. De Oliveira, C.E. Dykstra, Weakly bonded clusters of H2S, J. Mol. Struct. THEOCHEM 362 (1996) 275–282, https://doi.org/10.1016/0166-1280(95)04429-9.

[31] J.M. Hermida-Ramón, E.M. Cabaleiro-Lago, J. Rodríguez-Otero, Theoretical characterization of structures and energies of benzene- (H2S) n and (H2S) n (n=1–4) clusters, J. Chem. Phys. 122 (2005) 4–8, https://doi.org/10.1063/1.1901566.

[32] P. Soulard, B. Tremblay, Vibrational study in neon matrix of H2S-H2O, H2S-(H2O)2, and (H2S)2-H2O complexes. Identification of the two isomers: HOH-SH2 (H2O proton donor) and HSH-OH2 (H2S proton donor), J. Chem. Phys. 151 (2019) 124308, https://doi.org/10.1063/1.5120572.

[33] N. Rekik, A. Velcescu, P. Blaise, O. Henri-Rousseau, Spectral density of H-bonds. II. Intrinsic anharmonicity of the fast mode within the strong anharmonic coupling theory, Chem. Phys. 273 (2001) 11–37, https://doi.org/10.1016/S0301-0104(01)00470-0.

[34] N. Rekik, H. Ghalla, N. Issaoui, B. Oujia, M.J. Wójcik, Infrared spectral density of hydrogen bonds within the strong anharmonic coupling theory: quadratic dependence of the angular frequency and the equilibrium position of the fast mode, J. Mol. Struct. THEOCHEM 821 (2007) 58–70, https://doi.org/10.1016/j.theochem.2007.06.025.

[35] N. Rekik, N. Issaoui, H. Ghalla, B. Oujia, M.J. Wójcik, IR spectral density of H-bonds. Both intrinsic anharmonicity of the fast mode and the H-bond bridge. Part I: anharmonic coupling parameter and temperature effects, J. Mol. Struct. Theochem. 821 (2007) 9–21, https://doi.org/10.1016/j.theochem.2007.06.016.

[36] M.E.A. Benmalti, A. Krallafa, N. Rekik, M. Belhakem, Theoretical study of the νO-H IR spectra for the hydrogen bond dimers from the polarized spectra of glutaric and 1-naphthoic acid crystals: Fermi resonances effects, Spectrochim. Acta A Mol. Biomol. Spectrosc. 74 (2009) 58–66, https://doi.org/10.1016/j.saa.2009.05.005.

[37] N. Rekik, H.T. Flakus, A. Jarczyk-Jędryka, F. Abdulaziz Al-Agel, M. Daouahi, P.G. Jones, J. Kusz, M. Nowak, Elucidating the Davydov-coupling mechanism in hydrogen bond dimers: experimental and theoretical investigation of the polarized IR spectra of 3-thiopheneacetic and 3-thiopheneacrylic acid crystals, J. Phys. Chem. Solids 77 (2015) 68–84, https://doi.org/10.1016/j.jpcs.2014.10.008.

[38] K. Belhayara, D. Chamma, O. Henri-Rousseau, Infrared spectra of weak H-bonds: Fermi resonances and intrinsic anharmonicity of the H-bond bridge, J. Mol. Struct. 648 (2003) 93–106, https://doi.org/10.1016/S0022-2860(02)00618-X.

[39] N. Rekik, F.A. Al-Agel, H.T. Flakus, Davydov coupling as a factor influencing the H-bond IR signature: computational study of the IR spectra of 3-thiopheneacrylic acid crystal, Chem. Phys. Lett. 647 (2016) 107–113, https://doi.org/10.1016/j.cplett.2016.01.042.

[40] D. Chamma, O. Henri-Rousseau, IR theory of weak H-bonds: Davydov coupling, Fermi resonances and direct relaxations. I. Basis equations within the linear response theory, Chem. Phys. 248 (1999) 53–70, https://doi.org/10.1016/S0301-0104(99)00235-9.

[41] E.M. Mas, R. Bukowski, K. Szalewicz, G.C. Groenenboom, P.E.S. Wormer, A. van der Avoird, Water pair potential of near spectroscopic accuracy. I. Analysis of potential surface and virial coefficients, J. Chem. Phys. 113 (2000) 6687–6701, https://doi.org/10.1063/1.1311289.

[42] C. Leforestier, R. Van Harrevelt, A. Der Van Avoird, Vibration-rotation-tunneling levels of the water dimer from an ab initio potential surface with flexible monomers, J. Phys. Chem. A 113 (2009) 12285–12294, https://doi.org/10.1021/jp9020257.

[43] R.C. Cohen, R.J. Saykally, Vibration-rotation-tunneling spectroscopy of the van der Waals bond: a new look at intermolecular forces, J. Phys. Chem. 96 (1992) 1024–1040, https://doi.org/10.1021/j100182a006.

[44] N. Goldman, R. Fellers, M. Brown, L. Braly, C. Keoshian, C. Leforestier, R. Saykally, Spectroscopic determination of the water dimer intermolecular potential-energy surface, J. Chem. Phys. 116 (2002) 10148, https://doi.org/10.1063/1.1476932.

[45] C. Leforestier, F. Gatti, R.S. Fellers, R.J. Saykally, Determination of a flexible (12D) water dimer potential via direct inversion of spectroscopic data, J. Chem. Phys. 117 (2002) 8710–8722, https://doi.org/10.1063/1.1514977.

[46] R.E.A. Kelly, J. Tennyson, G.C. Groenenboom, A. van der Avoird, Water dimer vibration-rotation tunnelling levels from vibrationally averaged monomer wavefunctions, J. Quant. Spectrosc. Radiat. Transf. 111 (2010) 1262–1276, https://doi.org/10.1016/j.jqsrt.2010.01.033.

[47] R. Bukowski, K. Szalewicz, G.C. Groenenboom, A. Van Der Avoird, Predictions of the properties of water from first principles, Science (80-. ) 315 (2007) 1249–1252, https://doi.org/10.1126/science.1136371.

[48] R.S. Fellers, L.B. Braly, R.J. Saykally, C. Leforestier, Fully coupled six-dimensional calculations of the water dimer vibration-rotation-tunneling states with split Wigner pseudospectral approach. II. Improvements and tests of additional potentials, J. Chem. Phys. 110 (1999) 6306–6318, https://doi.org/10.1063/1.478535.

[49] C. Leforestier, K. Szalewicz, A. Van Der Avoird, Spectra of water dimer from a new ab initio potential with flexible monomers, J. Chem. Phys. 137 (2012) https://doi.org/10.1063/1.4722338.

[50] G.T. Fraser, (H2o)2: spectroscopy, structure and dynamics, Int. Rev. Phys. Chem. 10 (1991) 189–206, https://doi.org/10.1080/01442359109353257.

[51] C. Leforestier, L.B. Braly, K. Liu, M.J. Elrod, R.J. Saykally, Fully coupled six-dimensional calculations of the water dimer vibration-rotation-tunneling states with a split Wigner pseudo spectral approach, J. Chem. Phys. 106 (1997) 8527–8544, https://doi.org/10.1063/1.473908.

[52] R. Bukowski, K. Szalewicz, G.C. Groenenboom, A. Van Der Avoird, Polarizable interaction potential for water from coupled cluster calculations. I. Analysis of dimer potential energy surface, J. Chem. Phys. 128 (2008) https://doi.org/10.1063/1.2832746.

[53] W.C. Lane, T.H. Edwards, J.R. Gillis, F.S. Bonomo, F.J. Murcray, Analysis of ν2 of H2S, J. Mol. Spectrosc. 95 (1982) 365–380, https://doi.org/10.1016/0022-2852(82)90136-9.

[54] L.L. Strow, Measurement and analysis of the ν2 band of H2S: comparison among several reduced forms of the rotational Hamiltonian, J. Mol. Spectrosc. 97 (1983) 9–28, https://doi.org/10.1016/0022-2852(83)90334-X.

[55] O.N. Ulenikov, A.B. Malikova, M. Koivusaari, S. Alanko, R. Anttila, High resolution vibrational–rotational spectrum of H2S in the region of the ν2 fundamental band, J. Mol. Spectrosc. 176 (1996) 229–235, https://doi.org/10.1006/jmsp.1996.0082.

[56] S.S. Nabiev, L.A. Palkina, V.I. Starikov, IR spectra and dipole moment function of the H2S molecule in the gas and liquid phases, Russ. J. Phys. Chem. B 7 (2013) 721–733, https://doi.org/10.1134/S1990793113060079.

[57] L.R. Brown, J.A. Crisp, D. Crisp, O.V. Naumenko, M.A. Smirnov, L.N. Sinitsa, A. Perrin, The absorption spectrum of H2S between 2150 and 4260 cm−1: analysis of the positions and intensities in the first (2ν2, ν1, and ν3) and second (3ν2, ν1 + ν2, and ν2 + ν3) triad regions, J. Mol. Spectrosc. 188 (1998) 148–174, https://doi.org/10.1006/jmsp.1997.7501.

[58] E. Isoniemi, M. Pettersson, L. Khriachtchev, J. Lundell, M. Räsnen, Infrared spectroscopy of H2S and SH in rare-gas matrixes, J. Phys. Chem. A 103 (1999) 679–685, https://doi.org/10.1021/jp9838893.

[59] A.J. Barnes, J.D.R. Howells, Infra-red cryogenic studies. Part 7—hydrogen sulphide in matrices, J. Chem. Soc. Faraday Trans. 2 Mol. Chem. Phys. 68 (1972) 729–736, https://doi.org/10.1039/F29726800729.

[60] A.J. Barnes, R.M. Bentwood, M.P. Wright, Molecular complexes between hydrogen sulphide and water studied by matrix isolation infrared spectroscopy, J. Mol. Struct. 118 (1984) 97–102, https://doi.org/10.1016/0022-2860(84)85184-4.

[61] B. Nelander, Infrared spectrum of the water–hydrogen sulfide complex, J. Chem. Phys. 69 (1978) 3870–3871, https://doi.org/10.1063/1.437026.

[62] E.L. Woodbridge, T.L. Tso, M.P. Mcgrath, W.J. Hehre, E.K.C. Lee, Infrared-spectra of matrix-isolated monomeric and dimeric hydrogen-sulfide in solid O-2, J. Chem. Phys. 85 (1986) 6991–6994, https://doi.org/10.1063/1.451386.

[63] F. Huisken, M. Kaloudis, A. Kulcke, Infrared spectroscopy of small size-selected water clusters, J. Chem. Phys. 104 (1996) 17–25, https://doi.org/10.1063/1.470871.

[64] A.J. Tursi, E.R. Nixon, Infrared spectra of matrix-isolated hydrogen sulfide in solid nitrogen, J. Chem. Phys. 53 (1970) 518–521, https://doi.org/10.1063/1.1674019.

[65] L. Ciaffoni, B.L. Cummings, W. Denzer, R. Peverall, S.R. Procter, G.a.D. Ritchie, Line strength and collisional broadening studies of hydrogen sulphide in the 1.58 μm region using diode laser spectroscopy, Appl. Phys. B Lasers Opt. 92 (2008) 627–633, https://doi.org/10.1007/s00340-008-3119-y.

[66] J.E. Lowder, La. Kennedy, K.G.P. Sulzmann, S.S. Penner, Spectroscopic studies of hydrogen bonding in H2S, J. Quant. Spectrosc. Radiat. Transf. 10 (1970) 17–23, https://doi.org/10.1016/0022-4073(70)90126-3.

[67] E.A. Orabi, G. Lamoureux, Simulation of liquid and supercritical hydrogen sulfide and of alkali ions in the pure and aqueous liquid, J. Chem. Theory Comput. 10 (2014) 3221–3235, https://doi.org/10.1021/ct5002335.

[68] P.F. Fernandez, J.V. Ortiz, E.A. Walters, Calculations on species relevant to the photoionization of the van der Waals molecule (H2S)2, J. Chem. Phys. 84 (1986) 1653–1658, https://doi.org/10.1063/1.450460.

[69] M. Albertí, A. Amat, A. Aguilar, F. Pirani, Molecular dynamics simulations of small clusters and liquid hydrogen sulfide at different thermodynamic conditions, J. Phys. Chem. A 120 (2016) 4749–4757, https://doi.org/10.1021/acs.jpca.5b11843.

[70] W.L. Jorgensen, Intermolecular potential functions and Monte Carlo simulations for liquid sulfur compounds, J. Phys. Chem. 90 (1986) 6379–6388, https://doi.org/10.1021/j100281a063.

[71] H. Tsujii, K. Takizawa, S. Koda, IR spectra of hydrogen bonding of H2S doped in Kr solids, Chem. Phys. 285 (2002) 319–326, https://doi.org/10.1016/S0301-0104(02)00833-9.

[72] J.A. Pople, B.T. Luke, M.J. Frisch, J.S. Binkley, Theoretical thermochemistry. 1. Heats of formation of neutral AHn molecules (A = Li to Cl), J. Phys. Chem. 89 (1985) 2198–2203, https://doi.org/10.1021/j100257a013.

[73] S. Sarkar, M. Morwal, B. Bandyopadhyay, Cooperative nature of sulfur centered hydrogen bond: Investigation of (H2S) n (n = 2–4) clusters using an affordable yet accurate level of theory, Phys. Chem. Chem. Phys. 21 (2019) 25439–25448, https://doi.org/10.1039/c9cp05326c.

[74] A.B.M. de Aquino, L.A. Leal, V.H. Carvalho-Silva, R. Gargano, L.A. Ribeiro Junior, W.F. da Cunha, Krypton-methanol spectroscopic study: assessment of the complexation dynamics and the role of the van der Waals interaction, Spectrochim. Acta A Mol. Biomol. Spectrosc. 205 (2018) 179–185, https://doi.org/10.1016/j.saa.2018.06.110.

[75] H.V.R. Vila, L.A. Leal, A.L.A. Fonseca, R. Gargano, Calculation of the H2+ rovibrational energies and spectroscopic constants in the 2pπ, 3dσ, 4dσ, 4fπ, 4fσ, 5gσ, and 6iσ electronic states, Int. J. Quantum Chem. 112 (2012) 829–833, https://doi.org/10.1002/qua.23070.

[76] H.V. Rivera Vila, L.A. Leal, L.A. Ribeiro, J.B. Lopes Martins, G.M.E. Silva, R. Gargano, Spectroscopic properties of the H-2(+) molecular ion in the 8k pi, 9k sigma, 9l pi, 9l sigma and 10o sigma electronic states, J. Mol. Spectrosc. 273 (2012) 26–29, https://doi.org/10.1016/j.jms.2012.02.002.

[77] D.J. Frisch, M.J. Trucks, G.W. Schlegel, H.B. Scuseria, G.E. Robb, M.A. Cheeseman, J.R. Scalmani, G. Barone, V. Petersson, G.A. Nakatsuji, H. Li, X. Caricato, M. Marenich, A.V. Bloino, J. Janesko, B.G. Gomperts, R. Mennucci, B. Hratch, Gaussian 16, Revision B.01, 2016.

[78] J.F. Stanton, J. Gauss, L. Cheng, M.E. Harding, D.A. Matthews, P.G. Szalay, CFOUR, Coupled-Cluster techniques for Computational Chemistry, a quantum-chemical program package (n.d.).

[79] M. Kaupp, D. Danovich, S. Shaik, Chemistry is about energy and its changes: a critique of bond-length/bond-strength correlations, Coord. Chem. Rev. 344 (2017) 355–362.

[80] W. Lai, C. Li, H. Chen, S. Shaik, Hydrogen-abstraction reactivity patterns from A to Y: the valence bond way, Angew. Chem. Int. Ed. 51 (2012) 5556–5578.

[81] N. Kosar, K. Ayub, M.A. Gilani, T. Mahmood, Benchmark DFT studies on \ce{C-CN} homolytic cleavage and screening the substitution effect on bond dissociation energy, J Mol Model 25 (2019).

[82] M.D. Morse, Predissociation measurements of bond dissociation energies, Acc. Chem. Res. 52 (2018) 119–126.

[83] Z. Fang, M. Vasiliu, K.A. Peterson, D.A. Dixon, Prediction of bond dissociation energies/heats of formation for diatomic transition metal compounds: CCSD(T) works, J. Chem. Theory Comput. 13 (2017) 1057–1066.

[84] O.A. Stasyuk, R. Sedlak, C.F. Guerra, P. Hobza, Comparison of the DFT-SAPT and canonical EDA Schemes for the energy decomposition of various types of noncovalent interactions, J. Chem. Theory Comput. 14 (2018) 3440–3450.

[85] D.S. Levine, M. Head-Gordon, Energy decomposition analysis of single bonds within Kohn-Sham density functional theory, Proc. Natl. Acad. Sci. U. S. A. 114 (2017) 12649–12656.

[86] D. Cremer, E. Kraka, From molecular vibrations to bonding, chemical reactions, and reaction mechanism, Curr. Org. Chem. 14 (2010) 1524–1560, https://doi.org/10.2174/138527210793563233.

[87] W. Zou, R. Kalescky, E. Kraka, D. Cremer, Relating normal vibrational modes to local vibrational modes with the help of an adiabatic connection scheme, J. Chem. Phys. 137 (2012) 84114, https://doi.org/10.1063/1.4747339.

[88] W. Zou, D. Cremer, C2 in a box: determining its intrinsic bond strength for the X1Σg+ ground state, Chem. Eur. J. 22 (2016) 4087–4097.

[89] Z. Konkoli, D. Cremer, A new way of analyzing vibrational spectra. I. Derivation of adiabatic internal modes, Int. J. Quantum Chem. 67 (1998) 1–9 https://sites.smu.edu/dedman/catco/publications/pdf/IJQC_67_1_1998.pdf.

[90] Z. Konkoli, J.A. Larsson, D. Cremer, A new way of analyzing vibrational spectra. {II}. Comparison of internal mode frequencies, Int. J. Quant. Chem. 67 (1998) 11–27, https://doi.org/10.1002/(sici)1097-461x(1998)67:1<11::aid-qua2>3.0.co;2-1.

[91] E.B. Wilson, J.C. Decius, P.C. Cross, Molecular Vibrations. The Theory of Infrared and Raman Vibrational Spectra, McGraw-Hill, New York, 1955.

[92] E.B. Wilson Jr., A method of obtaining the expanded secular equation for the vibration frequencies of a molecule, J. Chem. Phys. 7 (1939) 1047.

[93] S. Califano, Vibrational States, Wiley, London, 1976.

[94] J.C. Decius, Compliance matrix and molecular vibrations, J. Chem. Phys. 38 (1963) 241.

[95] W. Zou, D. Cremer, Properties of local vibrational modes: the infrared intensity, Theor. Chem. Accounts 133 (2014) 1451, https://doi.org/10.1007/s00214-014-1451-3.

[96] Z. Konkoli, D. Cremer, A new way of analyzing vibrational spectra. {III}. Characterization of NORMAL vibrational modes in terms of internal vibrational modes, Int. J. Quantum Chem. 67 (1998) 29–40, https://doi.org/10.1002/(SICI)1097-461X (1998)67:1<29::AID-QUA3>3.0.CO;2-0.

[97] D. Cremer, J.A. Larsson, E. Kraka, New developments in the analysis of vibrational spectra on the use of adiabatic internal vibrational modes, in: C. Parkanyi (Ed.), Theor. Comput. Chem. Elsevier, Amsterdam 1998, pp. 259–327, https://doi.org/10.1016/s1380-7323(98)80012-5.

[98] R. Kalescky, E. Kraka, D. Cremer, Local vibrational modes of the formic acid dimer - the strength of the double H-bond, Mol. Phys. 111 (2013) 1497–1510, https://doi.org/10.1080/00268976.2013.796070.

[99] R. Kalescky, E. Kraka, D. Cremer, New approach to Tolman's electronic parameter based on local vibrational modes, Inorg. Chem. 53 (2013) 478–495, https://doi.org/10.1021/ic4024663.

[100] E. Kraka, J.A. Larsson, D. Cremer, Generalization of the badger rule based on the use of adiabatic vibrational modes, in: J. Grunenberg (Ed.), Comput. Spectrosc. Wiley, New York 2010, pp. 105–149, https://doi.org/10.1002/9783527633272.ch4.

[101] R. Kalescky, E. Kraka, D. Cremer, Identification of the strongest bonds in chemistry, J. Phys. Chem. A 117 (2013) 8981–8995, https://doi.org/10.1021/jp406200w.

[102] E. Kraka, D. Cremer, Characterization of CF bonds with multiple-bond character: bond lengths, stretching force constants, and bond dissociation energies, ChemPhysChem. 10 (2009) 686–698, https://doi.org/10.1002/cphc.200800699.

[103] E. Kraka, D. Setiawan, D. Cremer, Re-evaluation of the bond length–bond strength rule: the stronger bond is not always the shorter bond, J. Comput. Chem. 37 (2016) 130–142, https://doi.org/10.1002/jcc.24207.

[104] D. Setiawan, D. Sethio, D. Cremer, E. Kraka, From strong to weak NF bonds: on the design of a new class of fluorinating agents, Phys. Chem. Chem. Phys. 20 (2018) 23913–23927, https://doi.org/10.1039/c8cp03843k.

[105] M.Z. Makoś, M. Freindorf, D. Sethio, E. Kraka, New insights into Fe-H2 and Fe-H-bonding of a [NiFe] hydrogenase mimic - a local vibrational mode study, Theor. Chem. Acc. 138 (2019)https://doi.org/10.1007/s00214-019-2463-9.

[106] V. Oliveira, E. Kraka, D. Cremer, The intrinsic strength of the halogen bond: electrostatic and covalent contributions described by coupled cluster theory, Phys. Chem. Chem. Phys. 18 (2016) 33031–33046, https://doi.org/10.1039/c6cp06613e.

[107] V. Oliveira, E. Kraka, D. Cremer, Quantitative assessment of halogen bonding utilizing vibrational spectroscopy, Inorg. Chem. 56 (2016) 488–502, https://doi.org/10.1021/acs.inorgchem.6b02358.

[108] V. Oliveira, D. Cremer, Transition from metal-ligand bonding to halogen bonding involving a metal as halogen acceptor: a study of Cu, Ag, Au, Pt, and Hg complexes, Chem. Phys. Lett. 681 (2017) 56–63, https://doi.org/10.1016/j.cplett.2017.05.045.

[109] V. Oliveira, D. Cremer, E. Kraka, The many facets of chalcogen bonding: described by vibrational spectroscopy, J. Phys. Chem. A 121 (2017) 6845–6862, https://doi.org/10.1021/acs.jpca.7b06479.

[110] V. Oliveira, E. Kraka, Systematic coupled cluster study of noncovalent interactions involving halogens, chalcogens, and pnicogens, J. Phys. Chem. A 121 (2017) 9544–9556, https://doi.org/10.1021/acs.jpca.7b10196.

[111] D. Setiawan, E. Kraka, D. Cremer, Hidden bond anomalies: the peculiar case of the fluorinated amine chalcogenides, J. Phys. Chem. A 119 (2015) 9541–9556, https://doi.org/10.1021/acs.jpca.5b05157.

[112] D. Setiawan, E. Kraka, D. Cremer, Strength of the pnicogen bond in complexes involving group VA elements N, P, and As, J. Phys. Chem. A 119 (2014) 1642–1656, https://doi.org/10.1021/jp508270g.

[113] D. Setiawan, E. Kraka, D. Cremer, Description of pnicogen bonding with the help of vibrational spectroscopy-the missing link between theory and experiment, Chem. Phys. Lett. 614 (2014) 136–142, https://doi.org/10.1016/j.cplett.2014.09.030.

[114] D. Setiawan, D. Cremer, Super-pnicogen bonding in the radical anion of the fluorophosphine dimer, Chem. Phys. Lett. 662 (2016) 182–187, https://doi.org/10.1016/j.cplett.2016.09.028.

[115] D. Sethio, V. Oliveira, E. Kraka, Quantitative assessment of tetrel bonding utilizing vibrational spectroscopy, Molecules. 23 (2018) 2763, https://doi.org/10.3390/molecules23112763.

[116] R. Kalescky, W. Zou, E. Kraka, D. Cremer, Local vibrational modes of the water dimer – comparison of theory and experiment, Chem. Phys. Lett. 554 (2012) 243–247, https://doi.org/10.1016/j.cplett.2012.10.047.

[117] Y. Tao, W. Zou, J. Jia, W. Li, D. Cremer, Different ways of hydrogen bonding in water - why does warm water freeze faster than cold water? J. Chem. Theory Comput. 13 (2016) 55–76, https://doi.org/10.1021/acs.jctc.6b00735.

[118] M. Freindorf, E. Kraka, D. Cremer, A comprehensive analysis of hydrogen bond interactions based on local vibrational modes, Int. J. Quantum Chem. 112 (2012) 3174–3187, https://doi.org/10.1002/qua.24118.

[119] Y. Tao, W. Zou, D. Sethio, N. Verma, Y. Qiu, C. Tian, D. Cremer, E. Kraka, In situ measure of intrinsic bond strength in crystalline structures: local vibrational mode theory for periodic systems, J. Chem. Theory Comput. 15 (2019) 1761–1776, https://doi.org/10.1021/acs.jctc.8b01279.

[120] E. Kraka, W. Zou, M. Filatov, Y. Tao, J. Grafenstein, D. Izotov, J. Gauss, Y. He, A. Wu, Z. Konkoli, V. Polo, L. Olsson, Z. He, D. Cremer, COLOGNE2019, 2019.

[121] D. Cremer, E. Kraka, Chemical bonds without bonding electron density — does the difference electron-density analysis suffice for a description of the chemical bond? Angew. Chemie Int. Ed. Engl. 23 (1984) 627–628, https://doi.org/10.1002/anie.198406271.

[122] T.A. Keith, AIMAll, TK Gristmill Software, 2017.

[123] J.N. Murrell, S. Carter, S.C. Farantos, P. Huxley, A.J.C. Varandas, Molecular Potential Energy Functions, J. Wiley, New York, NY, 1984.

[124] M.J.D. Powell, An efficient method for finding the minimum of a function of several variables without calculating derivatives, Comput. J. 7 (1964) 155–162, https://doi.org/10.1093/comjnl/7.2.155.

[125] J.L. Dunham, The energy levels of a rotating vibrator, Phys. Rev. 41 (1932) 721–731, https://doi.org/10.1103/PhysRev.41.721.

[126] J.J. Soares Neto, C. S, Numerical generation of optimized discrete variable representations, Brazilian J. Phys. 28 (1998) 1–11, https://doi.org/10.1590/S0103-97331998000100001.

[127] E.N.C. Paura, W.F. da Cunha, P.H. de Oliveira Neto, G.M. e Silva, J.B.L. Martins, R. Gargano, Vibrational and electronic structure analysis of a carbon dioxide interaction with functionalized single-walled carbon nanotubes, J. Phys. Chem. A 117 (2013) 2854–2861, https://doi.org/10.1021/jp312622s.

[128] H.V.R. Vila, L.A. Leal, J.B.L. Martins, D. Skouteris, G.M.E. Silva, R. Gargano, The H + Li 2 bimolecular exchange reaction: dynamical and kinetic properties at J = 0, J. Chem. Phys. 136 (2012) 134319, https://doi.org/10.1063/1.3700164.

[129] N.B. Slater, The rates of unimolecular reactions in gases, Math. Proc. Cambridge Philos. Soc. 35 (1939) 56–69, https://doi.org/10.1017/S0305004100020739.

[130] K.J. Laidler, Theories of Chemical Reaction Rates, McGraw-Hill, New York, NY, 1969.